journal of the mechanical behavior of biomedical materials 157 (2024) 106639

Contents lists available at ScienceDirect

Journal of the Mechanical Behavior of Biomedical Materials

journal homepage: www.elsevier.com/locate/jmbbm

Research paper

Dynamic biaxial loading of vascular smooth muscle cell seeded tissue equivalents

Daniel Paukner [a,b,c,1], Isabella R. Jennings [c,1], Christian J. Cyron [a,b], Jay D. Humphrey [c,*]

[a] Institute for Continuum and Material Mechanics, Hamburg University of Technology, Hamburg, Germany
[b] Institute of Material Systems Modeling, Helmholtz-Zentrum Hereon, Geesthacht, Germany
[c] Department of Biomedical Engineering, Yale University, New Haven, CT, USA

ARTICLE INFO

Keywords:
Tissue engineering
Tensional homeostasis
Cell–matrix interaction
Biaxial testing
Cell-seeded collagen gels
Mechanobiology

ABSTRACT

An intricate reciprocal relationship exists between adherent synthetic cells and their extracellular matrix (ECM). These cells deposit, organize, and degrade the ECM, which in turn influences cell phenotype via responses that include sensitivity to changes in the mechanical state that arises from changes in external loading. Collagen-based tissue equivalents are commonly used as simple but revealing model systems to study cell–matrix interactions. Nevertheless, few quantitative studies report changes in the forces that the cells establish and maintain in such gels under dynamic loading. Moreover, most prior studies have been limited to uniaxial experiments despite many soft tissues, including arteries, experiencing multiaxial loading *in vivo*. To begin to close this gap, we use a custom biaxial bioreactor to subject collagen gels seeded with primary aortic smooth muscle cells to different biaxial loading conditions. These conditions include cyclic loading with different amplitudes as well as different mechanical constraints at the boundaries of a cruciform sample. Irrespective of loading amplitude and boundary condition, similar mean steady-state biaxial forces emerged across all tests. Additionally, stiffness-force relationships assessed via intermittent equibiaxial force–extension tests showed remarkable similarity for ranges of forces to which the cells adapted during periods of cyclic loading. Taken together, these findings are consistent with a load-mediated homeostatic response by vascular smooth muscle cells.

1. Introduction

Many cell types are embedded *in vivo* within a three-dimensional extracellular matrix (ECM), a network of constituents that often includes different fibrillar collagens and proteoglycans as well as elastic fibers (Hynes and Naba, 2012). Besides endowing tissues with overall structural support, the ECM provides biochemical and biomechanical cues to resident and infiltrating cells. Changes in the composition, properties, and mechanical state of the ECM can thus influence diverse cell behaviors (Lukashev, 1998; Wells, 2008), including differentiation (Engler et al., 2006), proliferation (Klein et al., 2009), migration (Wolf et al., 2013), and survival (Wang et al., 2000). Cell–matrix interactions are typically dictated by mechanotransduction in development, health, and disease (Humphrey et al., 2014; Yamada et al., 2022).

Reduced model systems called tissue equivalents were introduced decades ago to simplify the study of cell–matrix interactions (Bell et al., 1979). Most tissue equivalents are based on collagen hydrogels, as collagen is the predominant structural protein in mammals. Even basic unloaded and unconstrained models have proven useful for studying how cells remodel the ECM, often by compacting initially low-stress isotropic gels (Redden and Doolin, 2003; Simon et al., 2014). More complex experimental systems can subject uniaxial cell-seeded collagen gels to static (Brown et al., 1998; Ezra et al., 2010; Hu et al., 2013) or dynamic (Lee et al., 2018; Walker et al., 2020; Wille et al., 2006) loading. Some of these devices can also measure the forces generated by the embedded cells. This led to the seminal finding of tensional homeostasis, the phenomenon whereby cells appear to establish and maintain a preferred state of tension (force per length) or stress (force per area), which can be maintained even when external perturbations (displacements or forces) are imposed (Brown et al., 1998).

Yet, because most soft tissues are subjected *in vivo* to multiaxial loading or constraints, biaxial bioreactors are necessary to mimic these conditions more closely. For example, vascular smooth muscle cells (VSMCs) are crucial for ensuring proper function of the aorta through their responses to changes in mechanical loading. VSMC responses include changes in the deposition, organization, and degradation of their ECM. Under normal conditions, VSMCs in many arteries (including the

* Corresponding author.
E-mail addresses: daniel.paukner@tuhh.de (D. Paukner), jay.humphrey@yale.edu (J.D. Humphrey).
[1] These authors contributed equally.

https://doi.org/10.1016/j.jmbbm.2024.106639
Received 26 March 2024; Received in revised form 18 June 2024; Accepted 18 June 2024
Available online 22 June 2024

descending thoracic aorta and abdominal aorta) experience a cyclic circumferential stretch caused by the pulsatile distension of the vessel during each cardiac cycle but little to no cyclic axial stretch. The associated cyclic axial stress yet appears to contribute significantly to aortic homeostasis and remodeling (Humphrey et al., 2009); indeed, changes in axial loading can elicit rapid and dramatic responses (Gleason and Humphrey, 2005a).

Different types of biaxial bioreactors have been developed to mimic the multiaxial nature of the *in vivo* environment and to study effects of mechanical loading and boundary conditions by performing stress–strain tests on cell-seeded tissue equivalents. For example, Hu et al. (2013) compared effects of static equibiaxial and strip-biaxial loading on the mechanical properties of tissue equivalents whereas Lee et al. (2018) studied effects of dynamic cyclic equibiaxial loading. Other studies have quantified induced changes in the alignment of cells and ECM fibers in response to stretch (Chen et al., 2018; Gould et al., 2012) or sought to improve the mechanical properties of tissue-engineered constructs, particularly to yield better functionality (Mol et al., 2005; Seliktar et al., 2001; Shearn et al., 2007).

We previously developed a computer-controlled biaxial bioreactor that can measure cell-generated forces in response to prescribed static or dynamic boundary conditions imposed via four micro-stepper motors (Eichinger et al., 2020), with tests including uniaxial, strip-biaxial, equibiaxial, and non-equibiaxial stretching (Fig. A.10). Of importance herein, a strip biaxial protocol holds the sample at a constant overall stretch along one axis while cyclically stretching in the orthogonal axis, which resembles mechanical constraints experienced by VSMCs over a cardiac cycle in most segments of the aorta. We used this device to examine force generation by primary murine aortic SMCs subjected to dynamic loading conditions that are motivated by physiological conditions. Cruciform, VSMC-seeded collagen gels were subjected to two primary loading conditions. First, effects of increased biaxial stresses/stretches were examined using cyclic equibiaxial loading of different amplitudes. Second, effects of cyclic equibiaxial (biaxial stress and stretch) versus cyclic strip-biaxial (biaxial stress but not stretch) loading were examined while keeping the amplitude of the primary stretching the same. To the best of our knowledge, this is the first quantification and comparison of diverse types of cyclic loading of VSMC-seeded tissue equivalents, particularly using *in vivo* relevant conditions having implications to multiaxial tensional homeostasis.

2. Methods

2.1. Primary cell isolation and culture

Primary aortic SMCs of mesoderm lineage were isolated from the descending thoracic aorta, suprarenal abdominal aorta, and infrarenal abdominal aorta from ~13-week-old male C57BL/6J mice that were euthanized for a different study, with all live animal care and use approved by the Yale Institutional Animal Care and Use Committee. Toward this end, the aorta was excised from the left subclavian artery to the aorto-iliac bifurcation, cleaned, and subjected to an enzyme dispersion method to isolate the cells (Proudfoot and Shanahan, 2012). The digestion solution consisted of HBSS (with Ca^{2+} and Mg^{2+}, Gibco), collagenase type IV (1 mg/ml, Gibco), elastase (0.744 U/ml, Sigma-Aldrich), soybean trypsin inhibitor (1 mg/ml, Sigma-Aldrich), and penicillin-streptomycin (1% v/v, Gibco). Following partial digestion of the ECM for 10 min at room temperature, the aorta was transferred to a complete culture medium of 20% fetal bovine serum (FBS, Sigma-Aldrich) in DMEM (Sigma-Aldrich) for 2-3 min to neutralize the digestion solution. The adventitia was then removed using forceps, the wall was cut open, and the endothelial cell layer was denuded. The remaining medial layer was then sliced into small pieces and placed in an Eppendorf tube containing the same digestion solution. After 1 h of incubation at 37 °C to digest the ECM and disperse the cells, the cell suspension was neutralized again with complete medium before being centrifuged to collect the cell pellet for seeding onto fibronectin-coated culture plates. Aortas of five different mice were used and kept separate during the isolation and expansion process. Cells were stained for smooth muscle α-actin to confirm cell type, noting that separate adventitial-derived fibroblasts did not stain with smooth muscle α-actin.

The VSMCs were maintained in a humidified incubator at 5% CO_2 and 37 °C. Their first medium change occurred three days after seeding, then all other medium changes were performed every other day. The cells were expanded using complete medium until passage 3, when they were frozen using a freezing medium composed of 90% complete medium and 10% DMSO and transferred to liquid nitrogen for long-term storage.

2.2. Gel preparation

One week before each experiment, cells were thawed and seeded in collagen-coated (40 μg/ml) culture flasks and maintained in a humidified incubator at 5% CO_2 and 37 °C with 10% FBS in DMEM. The cells were starved 24 h prior to the experiment by reducing FBS to 2% to reduce cell proliferation and effects of growth factors and hormones.

Collagen gels were prepared following the protocol described in Eichinger et al. (2020). Briefly, 1.414 ml of 5X DMEM (Gibco), 0.676 ml of 10X reconstitution buffer (0.1 M NaOH and 20 mM HEPES, Sigma-Aldrich), and 0.852 ml of high concentration type I rat tail collagen (8.22 mg/mL, Corning) were mixed with 4.058 mL of complete medium containing 2% FBS. Gels were kept on ice during preparation to prevent premature polymerization of the collagen. In the VSMC-seeded collagen gels, the medium contained 2.45×10^6 cells, resulting in a final cell density of 0.35×10^6 cells/ml of gel. For all experiments, cells were at passage 4.

2.3. Biaxial mechanical testing

For testing in our biaxial bioreactor (Eichinger et al., 2020), the collagen gels were poured into a cruciform mold with four porous attachments to the loading system already in place (Fig. 1A). The gel polymerized for 30 min before filling the bioreactor bath with 80 mL of 2% FBS medium, after which the mold was removed. With the initially stress-free gel floating and attached to the force transducers, we initiated the computer-controlled loading protocol and began force measurement. Cell-generated forces were measured using two identical force transducers, one per stretching axis, each with a range of 0–5 mN (SI-H KG7, World Precision Instruments). Typical forces ranged from 0–1 mN. Overall displacements at the ends of the four arms of the cruciform samples were applied via four micro-stepper motors (Advanced Micro Systems), each with a resolution of approximately 1 μm. Prior and preliminary studies suggested that there was firm attachment of the gels within the porous attachments, with no slippage. See Eichinger et al. (2020) for further details on the experimental system.

All loading protocols were divided into the same three phases (see Fig. 1B). First, the gel was maintained in its original configuration for ~15 h to allow the cells to attach to the collagen matrix and establish steady-state values of biaxial force. Second, a quasi-static force–extension test was performed whereby the gel was subjected to a 10% equibiaxial stretch over 10 min and then returned to 0% stretch (the state achieved after the 15-h initialization phase) over 10 min, thus yielding a constant stretch rate of 1.67×10^{-4} s^{-1} (defined as change in overall length per reference length per time). Third, the gel was subjected to a seven-hour cycling period, with either equibiaxial or strip-biaxial stretching. These last two phases – force–extension test and cyclic loading – formed an experimental interval that was repeated seven times. Combined with the initialization phase and the force–extension tests, this results in a total computer-controlled duration of approximately 66 h per gel.

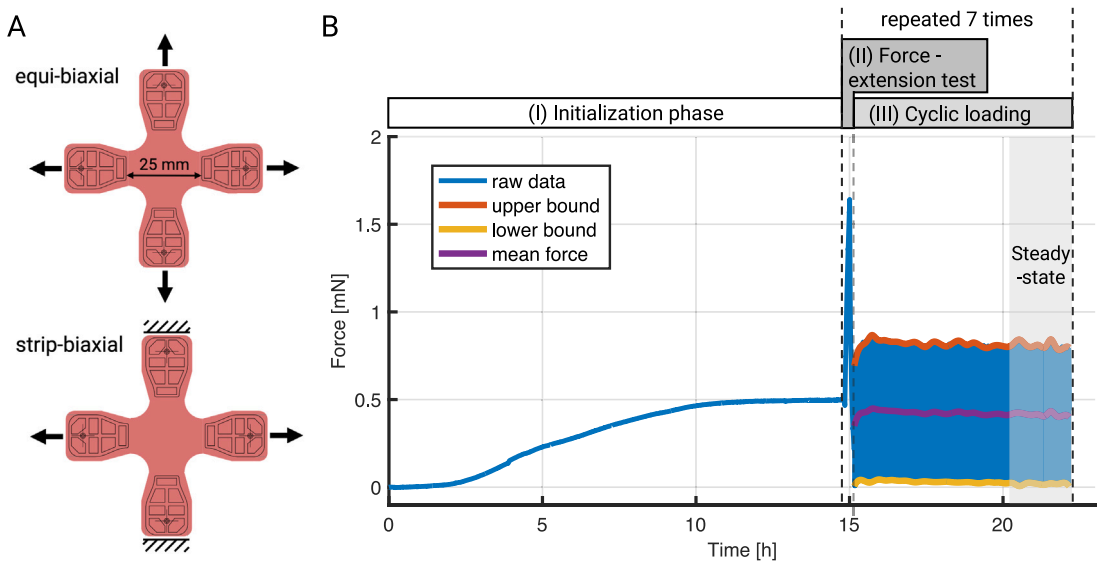

Fig. 1. Illustration of boundary conditions and loading protocols. (A) Equibiaxial (top) and strip-biaxial (bottom) loading conditions with porous fixtures at the ends of the four arms of the cruciform samples (pink) allowing the gels to be coupled easily to the four motor-controlled arms and two force transducers (one per axis). (B) The loading protocols consisted of three phases: (I) initialization, (II) force–extension testing, and (III) cyclic loading. The initialization phase lasted approximately 15 h and allowed the cells to attach to the collagen matrix and establish a steady-state biaxial force. The intermittent, quasi-static, equibiaxial force–extension tests consisted of a 10-min loading phase from 0% stretch to 10% superimposed stretch, then a 10-min unloading phase back to 0% stretch, each relative to the state established at the end of the initialization phase. The subsequent cyclic loading periods lasted seven hours each, with a force–extension test repeated after each cyclic loading period. To investigate effects of cyclic stretch amplitude, we compared 5% and 10% equibiaxial stretching; to examine the impact of different boundary conditions, a 5% strip-biaxial loading was included whereby one direction was cyclically stretched while the orthogonal direction remained at a fixed length. The last two phases – the force–extension test and cyclic loading – formed an interval that was repeated seven times. The blue line represents the preprocessed force measurements of one axis for a representative experiment; the orange, purple, and yellow curves correspond to the maximum, mean, and minimum force values during a cycling period, respectively, with force amplitude defined as the maximum minus minimum values.

Three different types of cyclic loading periods were compared. To examine effects of cycle amplitude, we performed 5% and 10% equibiaxial stretching protocols wherein both axes were stretched equally and simultaneously. Additionally, we performed strip-biaxial protocols wherein one axis was cyclically stretched 5% while the other was held at a fixed length, which allowed direct comparison to the 5% equibiaxial stretching protocol. The strip-biaxial test was chosen to mimic the mechanical conditions of the descending thoracic and abdominal aorta, in which there is little to no cyclic axial stretch but a consistent cyclic circumferential stretch due to the pulse wave originating from the heart (Bäck et al., 2013). It is important to note that both types of stretching protocols result, on average, in cyclic changes in biaxial stress while only the equibiaxial stretching protocol results, on average, in both cyclic stress and stretch (Humphrey et al., 2008). See Figs. A.11 and A.12 for additional qualitative insight into the stress and strain fields that can develop in the cruciform gels. The 5% cyclic loading was performed at a frequency of 0.5 Hz, whereas the 10% cyclic loading was performed at 0.25 Hz to maintain the stretch rate the same across protocols (0.05 s^{-1}). Albeit well less than the *in vivo* stretch rate in a mouse aorta, these rates are similar to those used in *ex vivo* studies on intact segments of the aorta (Ferruzzi et al., 2013). Control studies were repeated with acellular collagen gels under the same conditions. The loading conditions, the number of experiments performed per condition, and the abbreviations used in the following sections are summarized in Table 1.

2.4. Data (pre-)processing

The force transducers were sensitive to changes in temperature and humidity, which inevitably occur during the setup of the experiment when opening the incubator that housed the biaxial testing device. To eliminate this equilibration behavior during the initialization phase, we first computed the average forces for each transducer during the initialization phase of all acellular gels. These transducer-specific average values were then subtracted from the initialization phases of both the cellular and acellular experiments. For the time after the initialization phase, the force values were corrected with a constant value based on the last value of the transducer-specific average values. The preprocessed data were then analyzed using a custom MATLAB script. Briefly, the data were split into the three different periods: (I) initialization, (II) force–extension testing, and (III) cyclic loading. The amplitude, A_i, during each cyclic loading period, $i \in [1,7]$, was computed using MATLAB's *envelope()* method to extract upper (f_i^{high}) and lower (f_i^{low}) values, thus yielding the difference called force amplitude $A_i = f_i^{high} - f_i^{low}$. Mean force during each cyclic loading period was computed as $f_i = f_i^{low} + 0.5 \cdot A_i$. The different quantities – upper, lower, and mean force – are illustrated in Fig. 1B.

2.5. Data and statistical analysis

To compare effects of the different loading conditions quantitatively, we focused on average steady-state values of the mean forces and

Table 1
Summary of the three loading conditions for VSMC-seeded gels (for strip-biaxial tests, cyc denotes cyclic stretching, stat denotes the static axis), two of which were also used for acellular gels.

Testing protocol	Notation Protocol (n)	Axis-specific notation (Axis 1 vs. Axis 2)
Equibiaxial (E), 5% stretch amplitude	E5 (n = 5)	E5-1, E5-2
Equibiaxial (E), 10% stretch amplitude	E10 (n = 3)	E10-1, E10-2
Strip-biaxial (S), 5% stretch amplitude	S5 (n = 4)	S5-cyc, S5-stat
Equibiaxial (E), 5% stretch amplitude, Acellular	E5A (n = 4)	E5A-1, E5A-2
Strip-biaxial (S), 5% stretch amplitude, Acellular	S5A (n = 4)	S5A-cyc, S5A-stat

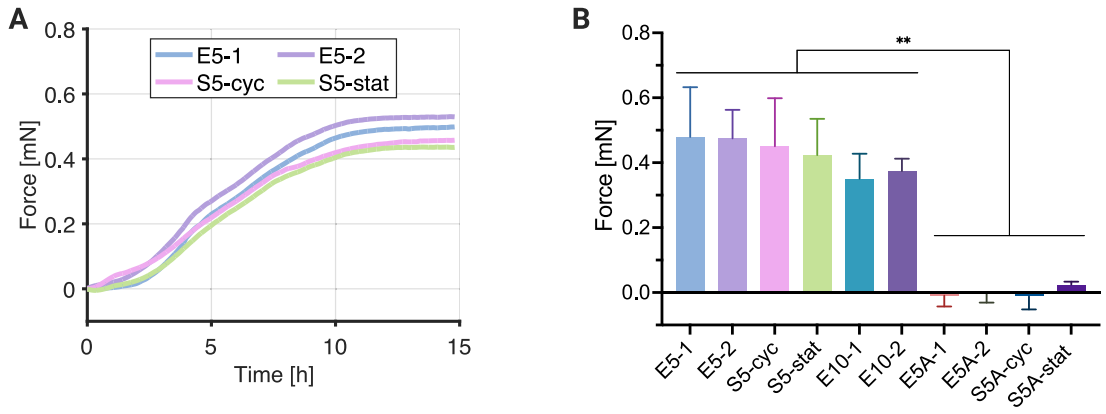

Fig. 2. Biaxial forces during and at the end of the ~15-h initialization phase. (A) Force evolution in the 1 and 2 directions for representative 5% equibiaxial (E5) and 5% strip-biaxial (S5) stretching experiments. (B) As expected, cellular gels generated significant biaxial forces during the initialization phase whereas acellular gels (denoted by A-1,2, cyc, or stat) generated negligible forces. Values of force on the ordinate represent axis-specific mean values calculated from the final two hours of initialization (**$p < 0.01$). See Table 1 for the nomenclature, with E5 or E10 denoting equibiaxial stretching of 5 or 10% and S5 denoting strip-biaxial stretching of 5% while the orthogonal direction remained static.

their amplitudes. The steady-state force at the end of the initialization phase was determined by averaging the measured values over the last two hours before beginning the first force–extension test. To compare cellular behaviors during cyclic loading, we used average values of force from the final two hours of each interval when both the mean forces and amplitudes had stabilized. A one-way or two-way repeated measures ANOVA with Tukey post-hoc testing was used for statistical comparisons of the different loading conditions. All statistical analysis was performed using GraphPad Prism 10, and results are reported as mean ± standard deviation unless noted otherwise.

3. Results

3.1. Initialization phase

Biaxial force generation was negligible in all acellular gels during the initialization phase. By contrast, there was significant force generation in all VSMC-seeded gels during this phase, with unremarkable differences between axis 1 and axis 2 across the various loading protocols (Fig. 2A). For this reason, average values of force (i.e., (axis 1 + axis 2)/2) are presented below for all equibiaxial experiments. Moreover, although these forces were slightly lower in the gels destined for 10% equibiaxial experiments (E10-1 and E10-2), these differences did not reach statistical significance when compared to all experiments involving cells (Fig. 2B). By contrast, mean forces observed in acellular gels were statistically different from those observed in cellular gels.

3.2. Cyclic loading periods

3.2.1. Consistent behavior within each loading period

Within each cyclic loading period, that is, the seven hours following each intermittent force–extension test, the cells tended to establish a new steady-state value of both force amplitude and mean force, irrespective of the cycle amplitude and boundary condition (Fig. 3). As expected, the initial force amplitude in the first interval of the E10 experiments was approximately twice as high as in the first interval of the E5 experiments (because the stretch was twice as high); it then gradually decreased and approached a value similar to the E5 experiments. Furthermore, in the E5 and S5 experiments, force amplitudes and mean forces tended to exhibit an initial increase during the first two to three hours of each cyclic loading period, suggesting further active cellular contributions. By contrast, in the E10 experiments, force amplitudes and mean forces remained largely stable over each seven-hour cyclic loading period, except during the first interval, where a decrease was observed. Compared to cellular gels, acellular gels exhibited smaller force amplitudes (Fig. B.13A) and mean forces (Fig. B.13B), each of which remained relatively constant during the experiments.

3.2.2. Steady-state force amplitudes

Analysis of the force amplitude during the final two hours of each cyclic loading period revealed that although E10 experiments tended to have the largest amplitudes, they were not statistically different from the E5 experiments (Fig. 4A). As expected, the static axis of the S5 experiment, denoted S5-stat, exhibited the smallest force amplitude and this difference was statistically significant compared with amplitudes across all intervals. A noteworthy trend observed in all VSMC-seeded gels was a decreasing amplitude from one interval to the next. In contrast, acellular amplitudes remained constant over time, albeit at a lower value (Fig. B.14A).

To assess in-plane coupling in the strip-biaxial experiments, we calculated the ratio of the force amplitude in the static axis to the amplitude in the cycled axis. In both cases, cellular and acellular, this ratio remained nearly constant over the seven intervals of study (Fig. 4B). However, the VSMC-seeded gels exhibited a significantly higher in-plane coupling compared to acellular gels.

3.2.3. Mean steady-state forces

Despite significant differences in steady-state force amplitudes in the cellular experiments (Fig. 4A), there were no statistically significant differences in steady-state mean forces across the different intervals and loading protocols (Fig. 5A). Of particular note, the force generated in the static axis of the strip-biaxial experiment closely approximated that generated in the cycled axis. The mean forces in the acellular experiments were lower than those in the VSMC-seeded gels (Fig. B.14B). Notably, both cellular and acellular experiments experienced a reduction in force from one interval to the next. This trend was more pronounced in cellular experiments, however.

To investigate whether there was a common underlying trend in the evolution of steady-state forces in the VSMC-seeded gels, we normalized the steady-state mean values by the force at the end of the initialization phase. This revealed that the behavior for all loading conditions was nearly identical (Fig. 5B), including for the E10 experiments that had a slightly lower mean force at the end of the initialization phase (Fig. 2B).

To quantify the absolute reduction in force during the experiments, we calculated the difference between the force in the initialization phase and the last interval (Fig. 6A). Cellular gels exhibited a considerably larger decrease in the average mean force when compared to acellular gels. Interestingly, the reduction in mean force appeared to be independent of the loading condition in cellular experiments, suggesting a common underlying cell-mediated mechanism. A statistically significant difference in mean force reduction became evident when comparing cellular (E5, S5) and acellular (E5A, S5A) experiments

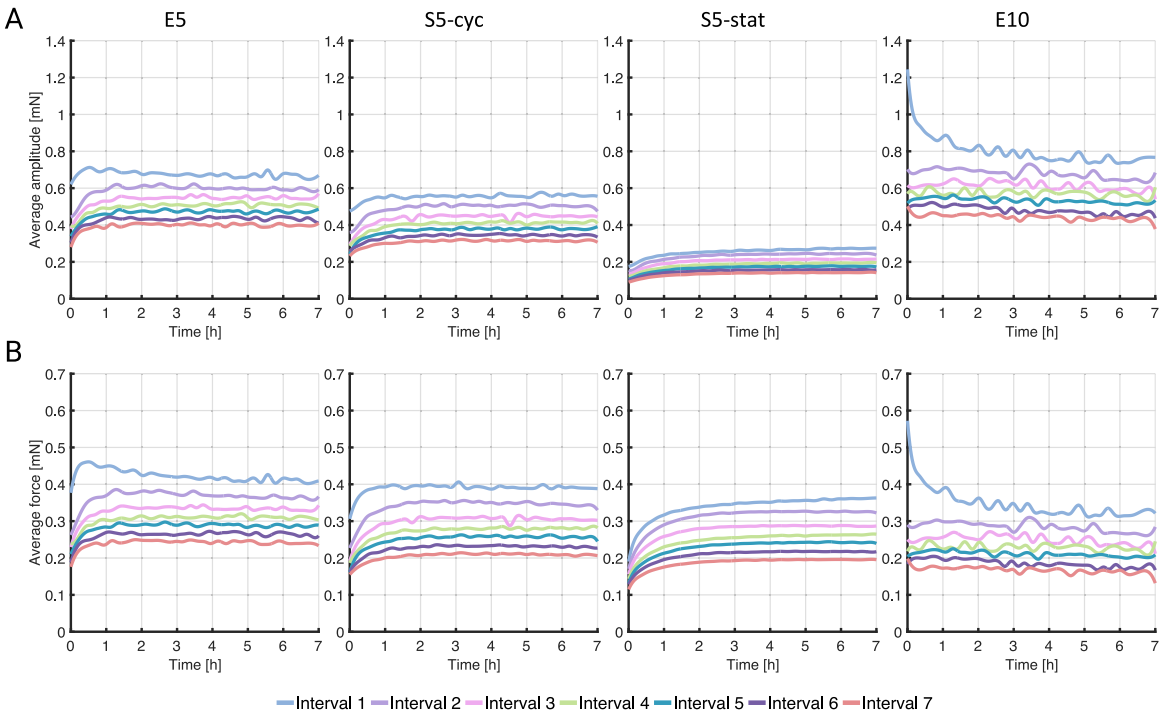

Fig. 3. Average values, that is, (axis 1 + axis 2)/2, of both force amplitude (A) and mean force (B) in VSMC-seeded gels during the seven, seven-hour cyclic loading periods. Referring to the nomenclature in Table 1, results are presented from left-to-right for the 3 experimental protocols for the VSMC-seeded gels, with periods 1–7 denoted by different colors: 1 – light blue, 2 – light purple, 3 – pink, 4 – green, 5 – blue, 6 – purple, 7 – red.

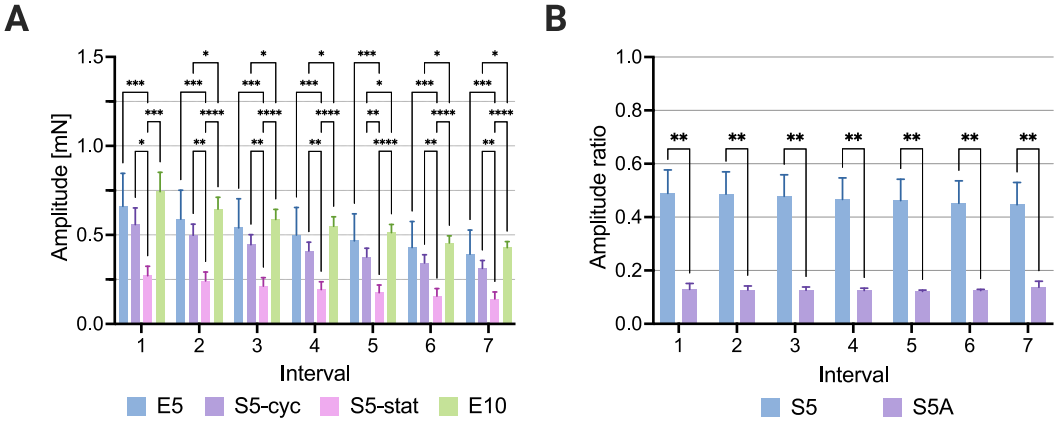

Fig. 4. Evolution of steady-state force amplitudes in VSMC-seeded collagen gels. (A) Steady-state amplitudes were calculated from the last two hours of each of the seven cyclic loading periods. Regardless of the magnitude of stretch imposed during cyclic loading, E5 and E10 showed similar steady-state amplitudes. The amplitude of the static axis in the strip-biaxial experiment was significantly different from all other amplitudes. (B) The ratio of the force amplitude in the static axis to that in the cycled axis was significantly higher in the cellular (S5) than in the acellular (S5A) strip-biaxial experiments, revealing an increased in-plane coupling in VSMC-seeded gels. The ratio remains nearly constant over time in both cases. (* $p < 0.05$, ** $p < 0.01$, *** $p < 0.001$, **** $p < 0.0001$).

(Fig. 6B). This eliminated transducer drift as the only cause as this should have affected both cellular and acellular experiments in a similar way. Additionally, transducer drift would be expected to show a continuous decrease in force, whereas the observed changes occurred in a step-like manner.

3.3. Equibiaxial force–extension tests

Before presenting results of the force–extension tests (FET), it is important to note that these tests do not necessarily begin from a stress-free configuration. Consequently, forces at zero imposed stretch are above zero for cellular gels (Fig. 7A–D) and either at or slightly below zero for acellular gels (Fig. 7E–H).

The first force–extension test in all cellular gels exhibited an almost linear relationship, though with a slight negative curvature in some cases indicating a stiffer behavior at low stretches and more compliant behavior at higher stretches (similar observations have been reported by others (Wagenseil et al., 2003; Wille et al., 2006) and is common in many elastomers). Nevertheless, the force-stretch relationship in the VSMC-seeded gels appeared nearly linear, while the acellular gels exhibited more of a nonlinear behavior. In both cases, cellular and acellular, there was no discernable difference between E5 and S5 experiments, with the static and cycled axes displaying similar behaviors during the equibiaxial force–extension tests. In the case of the E10 experiment, however, there was a notable reduction in stiffness (evidenced by the decreased slope of the curve) in the second force–extension test, which occurred after the first cyclic loading period. This

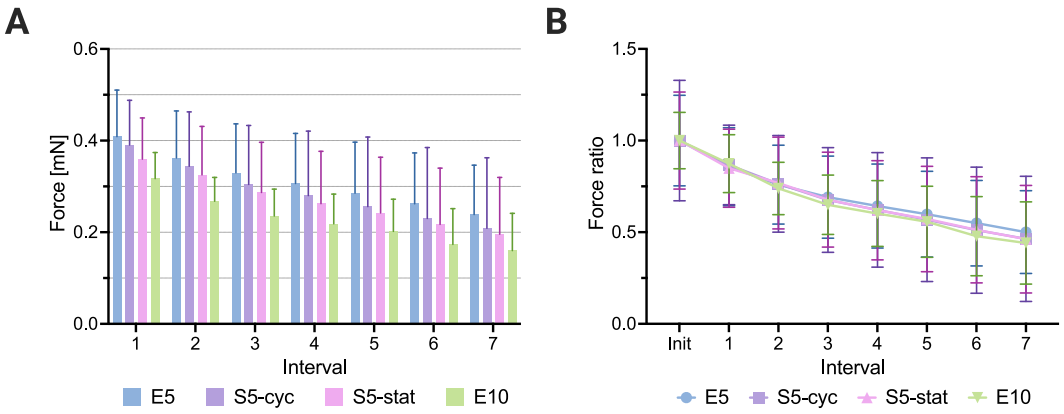

Fig. 5. Evolution of steady-state mean forces in VSMC-seeded collagen gels. (A) Average steady-state values of the mean forces were calculated from the last two hours of each loading interval. The steady-state forces decreased from interval to interval regardless of loading condition, and the forces of the static and cycled axes of the strip-biaxial experiment were comparable. (B) The force ratio was computed as the average force during the last two hours of an interval divided by the average force during the last two hours of the initialization phase. The graph reveals a similar trend for all loading conditions, potentially indicating a common underlying mechanism. Albeit not shown, a similar decrease was observed in pilot studies without intermediate force–extension testing.

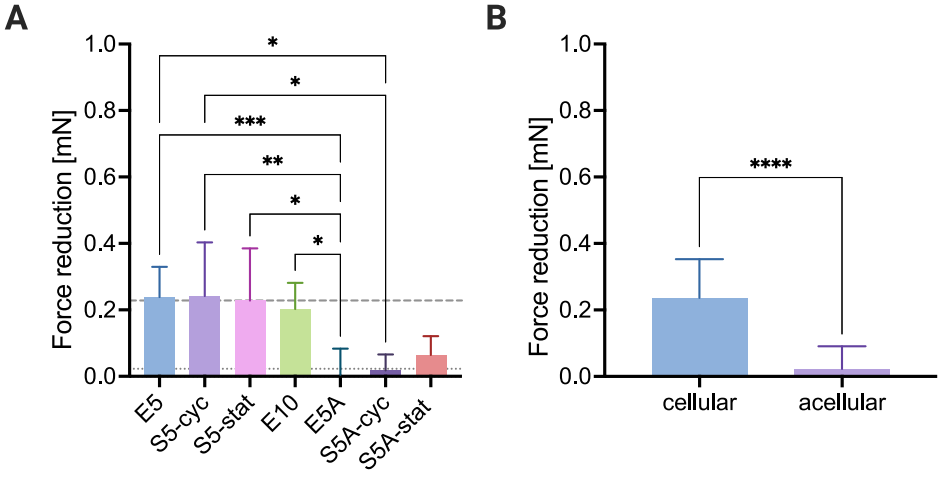

Fig. 6. Reduction in mean force from initialization phase to last cyclic loading interval. (A) Reduction in mean force between the end of the initialization phase and the end of the last (seventh) cyclic loading period for each loading condition. The dotted line represents the average value of all acellular experiments, and the dashed line represents the average value of all cellular experiments. (B) Comparing acellular (E5A, S5A) and cellular (E5, S5) experiments revealed a statistically significant difference (unpaired t-test). (*$p < 0.05$, **$p < 0.01$, *** $p < 0.001$, ****$p < 0.0001$).

reduction persisted in subsequent force–extension tests. Additionally, both acellular and cellular gels exhibited a continuous decrease in peak mean forces up to the 5th force–extension test, after which the force-stretch curves tended to stabilize.

Fig. 8A provides a visual representation of average loading and unloading curves for the second force–extension test of the E5 (blue curves) and E10 (green curves) experiments. The E10 experiment exhibited a distinct behavior compared to the other loading conditions, which is also evident from Fig. 7A–D. This was confirmed by fitting a linear relation to the loading curves to estimate the stiffness. Although the loading curves were not linear, this indicated a significant softening of the E10 gels (Fig. 8B).

Energy storage is determined as the area under the unloading curve (Fig. 8C), which remained nearly constant after the second force–extension test. Note that the E10 experiments exhibited significantly lower energy storage and dissipation than the other experiments after the first cyclic loading period. It is important to mention the difference in stored energy between the first E5 force–extension test and the first E10 force–extension test. Ideally, there should be no significant difference, but one possible explanation for this discrepancy could be the slight variation in the initialization force, which led to increased energy storage in the E5 experiments.

Dissipated energy is calculated as the area between the loading and unloading curves (Fig. 8D). This dissipation progressively decreased from one force–extension test to the next, as is common in tissue preconditioning. Experiments with a 10% cycle amplitude (E10) showed a significantly reduced energy dissipation from force–extension test 2 onward.

Fig. 9A plots mean stiffness vs. mean force generation for the first, third, fifth, and seventh force–extension tests (FET 1 through 7). Note the decreasing stiffness with increasing force in FET 1, which followed the 15-h static initialization phase. The subsequent tests, each following 7-h periods of cyclic loading, showed a marked difference: the nearly linear stiffness-force relationship changed its slope from negative (FET 1) to positive or zero (FETs 2–7) and separated into two linear regimes for the E5 and S5 experiments and one linear regime for the E10 experiment. It may be that E10 gels did not reach the same levels of force as the other loading conditions since they had already adapted to a 10% stretch during the cyclic loading periods. Regardless, the first linear regime was nearly identical for all loading conditions, whereas the second regime diverged slightly. The force at which the first linear regime transitioned into the second one coincided approximately with the maximum force that the gels had experienced during the last two hours of the previous cyclic loading period (Fig. 9B).

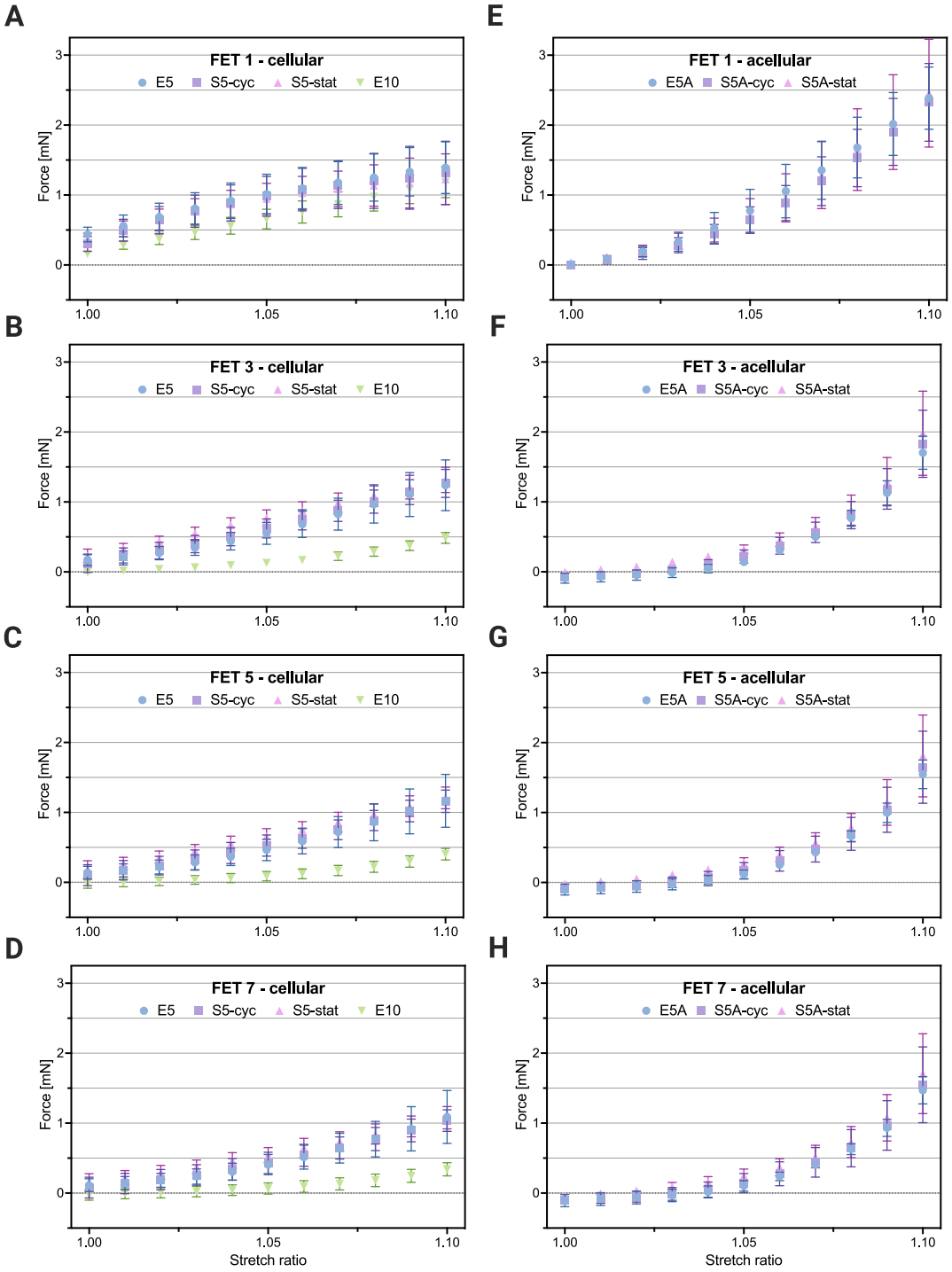

Fig. 7. Loading curves of selected intermediate force–extension tests (FETs). Shown are loading curves for FETs 1, 3, 5, and 7. The left column (A–D) shows results for VSMC-seeded gels and the right column (E–H) shows results for acellular gels. Acellular gels exhibited a more nonlinear force-stretch relationship, while VSMC-seeded gels exhibited a more linear behavior.

In contrast to the two distinct linear regimes observed in the VSMC-seeded gels, acellular gels exhibited a single nearly linear stiffness-force relationship, which did not change significantly during the course of the experiment (Fig. B.15).

4. Discussion

We quantified and compared how forces generated by primary aortic SMCs embedded within a collagenous tissue equivalent develop under different dynamic loading and boundary conditions in a biaxial setting. Whereas uniaxial tests are relatively easy to perform and interpret, they tend not to capture the complex multiaxial loading conditions that exist *in vivo*. Conversely, biaxial tests can better mimic *in vivo* conditions but are less easily performed and interpreted. Biaxial tests typically use rectangular or cruciform samples, each with associated advantages and disadvantages (Hu et al., 2009; Jhun et al., 2009; Thomopoulos et al., 2005). Important here, our measurements of overall biaxial forces in cruciform samples necessarily integrate cell-gel contributions from both the arms (which experience primarily

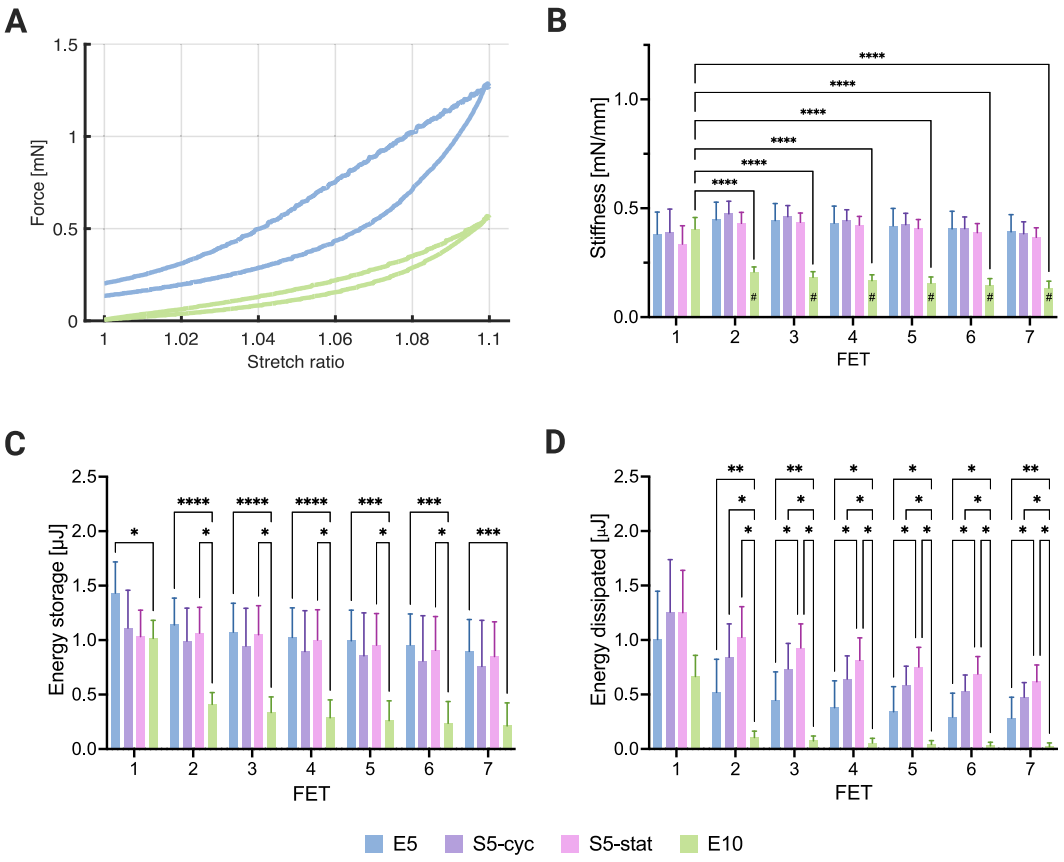

Fig. 8. Analysis of force–extension tests based on stiffness, energy storage, and energy dissipation. (A) Average loading and unloading curves of the second force–extension test (FET) for the E5 (blue) and E10 (green) experiments. (B) Stiffness estimation by simplified linear fit to loading curves. (C) The energy storage was computed as the area under the unloading curve for each loading condition. (D) The energy dissipated was computed as the area between the loading and unloading curves. (*$p < 0.05$, **$p < 0.01$, ***$p < 0.001$, ****$p < 0.0001$, #$p < 0.0001$ between E10 and all other loading conditions for the same force–extension test.)

uniaxial loading) and the central region (which experiences nonuniform biaxial stresses and strains) of the sample. Fig. A.10 shows stress–strain conditions under the relevant idealized situations, whereas Figs. A.11 and A.12 show possible nonuniform fields computed using finite elements for an illustrative initially homogeneous cruciform collagen gel. Although the evolving constitutive relation for a VSMC-seeded collagen gel is not known, similar qualitative results have been reported for simple Hookean (linear) and extended Mooney–Rivlin (mildly nonlinear) relations, that is, without superimposed cell-generated contributions. Results are shown here for the former for different values of Poisson's ratio for gels ranging from nearly incompressible ($\nu \sim 0.49$) to more compressible behaviors with less biaxial coupling ($\nu \sim 0.25$ or 0.10). Similar assumptions have been used previously (Barocas and Tranquillo, 1997; Raub et al., 2010) and likely capture qualitative trends. It is seen for a strip-biaxial case (with 1 the stretching axis and 2 the static axis) that, on average, the strains reach their target values of ~5% in the 1 direction and 0% in the 2 direction despite differences in the arms and central region. The predicted stresses were also as expected, on average, namely, overall tensile in both directions, with 1-direction stresses many-fold higher than 2-direction stresses. Yet, cell responses likely depend on local mechanical stimuli, not average states of strain and stress. The reported force measurements in our biaxial experiments necessarily represent the integrated responses by all cells, meaning cells that experienced different local stimuli. One would expect, however, that the integrated response should reflect an average of all cell responses. Given the continuing lack of understanding of how VSMCs respond to different levels and types of multiaxial stresses and strains, we also considered coordinate invariant values of the stress tensor. Spatial differences were less for the trace ($tr(\boldsymbol{\sigma})$) than for the magnitude ($\sqrt{tr(\boldsymbol{\sigma}\boldsymbol{\sigma}^T)}$) of the Cauchy stress, especially for equibiaxial stretching, remembering that the out-of-plane component of stress is zero.

Caveats notwithstanding, overall, the data suggested that, in a series of cyclic loading periods separated by force–extension tests, the cells established a new steady state level of biaxial force during each interval. This behavior is similar to prior observations in static experiments (Brown et al., 1998; Eichinger et al., 2020; Ezra et al., 2010) where cells tend to restore a preferred mechanical state when subjected to a single sustained external perturbation. It is especially interesting that the observed steady-state mean forces were similar across all protocols herein, regardless of the specific boundary conditions and amplitude of cyclic stretch over the range of 5 to 10% (Fig. 5B), and that the biaxial force generation in the two primary axes of the cruciform sample (f_1 and f_2) was similar. Conceptually, this implies that

$$\int (\sigma_{11}^{matrix} + \sigma_{11}^{cell}) dA = f_1 \approx f_2 = \int (\sigma_{22}^{matrix} + \sigma_{22}^{cell}) dA$$

where A is an appropriate cross-sectional area and we decomposed the stress into collagen gel (matrix) derived and VSMC (cell) generated contributions (cf. Barocas and Tranquillo (1997)). Since $\sigma_{11}^{matrix} \approx \sigma_{22}^{matrix}$ in an equibiaxial stretching test (which tends to preserve the original isotropy in the central region (Hu et al., 2009) and generate similar collagen fiber realignment in the uniaxial arms), this suggests that $\sigma_{11}^{cell} \approx \sigma_{22}^{cell}$ in equibiaxial stretching. By contrast, since $\sigma_{11}^{matrix} > \sigma_{22}^{matrix}$ in a strip-biaxial test, with 1 the stretching axis and 2 the static axis, this suggests that $\sigma_{22}^{cell} > \sigma_{11}^{cell}$. That is, it appears that differential cell-generated stresses were needed to yield the experimentally observed near equivalence of net force generation in the two primary directions independent of the type of loading conditions.

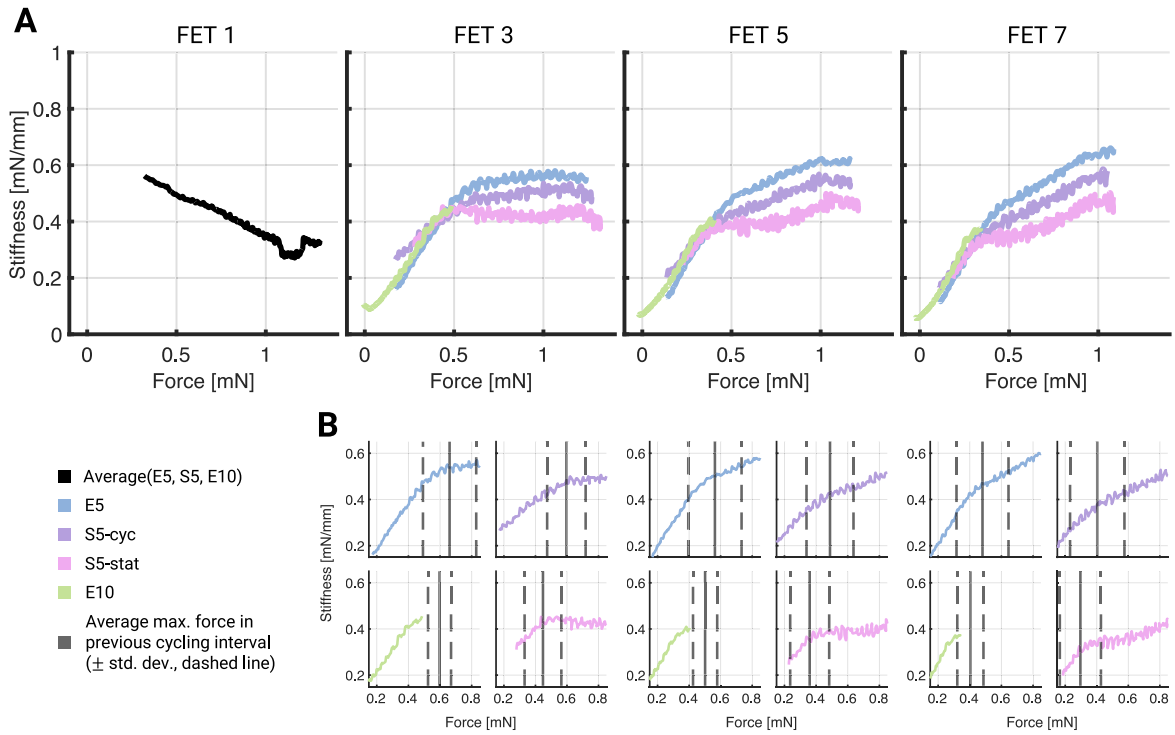

Fig. 9. Analysis of stiffness evolution for VSMC-seeded gels during consecutive force–extension tests (FETs). (A) Stiffness-force relationships for cell-seeded gels. All gels exhibited a similar behavior during the first test, which followed the initialization phase but changed significantly in the subsequent tests that followed the 7-h cyclic loading periods. Two distinct linear regimes appear to emerge for the E5 and S5 experiments, whereas one linear regime appears to hold for the E10 experiment over the forces imposed. Interestingly, there is a remarkable agreement in all loading conditions for small and medium forces. (B) Zoomed-in insets on the transition point from the first linear regime to the second one, including the average maximum force range the gels experienced during the last two hours of the previous cyclic loading interval. The transition point seems to be approximately in that range.

This experimental observation and conceptual consideration appear to be consistent with the cells seeking to establish and maintain a preferred range of forces (or tensions or stresses), irrespective of external boundary conditions. This implication also aligns with a previous observation that higher amplitude dynamic loading of uniaxial cell-seeded tissue equivalents does not lead to higher stresses after a few hours of cyclic loading (Wille et al., 2006), suggesting a cellular response aimed at maintaining a specific range of stresses. These authors hypothesized that cells achieve this regulation by adjusting their stiffness through modulation of the actin cytoskeleton. A recent study (Walker et al., 2020) confirmed this hypothesis by depolymerizing F-actin with Cytochalasin D. They proposed cytoskeletal remodeling, specifically rapid actin depolymerization, as the key mechanism by which cells adjust their stiffness and maintain a preferred mechanical state under dynamic loading defined by different strain amplitudes. Only with an intact actin cytoskeleton could cell stiffness adaptations occur, including softening. Moreover, they showed that tissue stiffness can be recovered when switching from large to small amplitudes during cyclic loading. This supports their observation that the stiffness adaptation was mainly cell-mediated, not a passive material response (such as, for example, the Mullins effect). Our experiments suggest further that, on average, cells may adapt their stiffness to maintain near-equal net steady-state forces (or tensions or stresses) despite different spatial distributions of stresses and strains.

This apparent force/tension/stress-mediated response seems to extend to the stiffness-force relationship of the cell-seeded tissue equivalents (Fig. 9). During equibiaxial force–extension tests, the average stiffness-force relationships agreed well within the force range experienced during the previous interval of cyclic loading for all tested conditions. This adaptation is not immediately apparent from force-stretch plots (Fig. 7A–D), as E10 experiments exhibited a significantly more compliant behavior. Nonetheless, this agreement diminished once forces exceeded the peak values experienced by the gels during the last two hours of the previous cyclic loading period; if stretched beyond this force, the stiffness either remained constant or increased at a lower rate. Again, the similar stiffness-force relationships for forces experienced during cyclic loading could suggest that cells not only adjust to maintain a preferred force/tension/stress but they also try to maintain a preferred stiffness or stiffness-force relationship. These two observations may not be independent, and further studies will be needed to explore and validate this relationship and find the direction of influence.

Another observation stems from the increase in force at the beginning of the cyclic loading periods in the E5 and S5 experiments (Fig. 3). The gels appeared to be initially too compliant, perhaps stimulating the cells to adjust to reach a preferred range of force/tension/stress. Interestingly, this behavior was absent in the E10 experiments. To explain this difference, we posit that these cells may have adapted to the cyclic 10% stretching by the end of the loading periods, evidenced by the steady-state mean forces and force amplitudes. Hence, during the following 10% stretch force–extension tests, the E10 cells would likely have had experienced the same forces/tensions/stresses to which they had adapted. As described before (Wille et al., 2006; Walker et al., 2020), cells can respond to higher forces by reducing their stiffness. Therefore, we hypothesize that the 10% stretch force–extension tests in the E5 and S5 experiments induced an active response by subjecting the cells to loads higher than previously experienced, triggering cellular adaptations leading to a reduced stiffness. This may also explain the reduced slope of the second linear regime for E5 and S5 experiments in the stiffness-force relationship once peak cycling forces were exceeded (Fig. 9B). For E10 experiments, perhaps there was only one linear regime in the stiffness-force relationship since the cells did not experience loads during force–extension tests that they had not experienced before. In this case, it seems reasonable that no further adaptation would occur; the cells would already be in the preferred state when cyclic loading resumed. Consequently, we suspect that the initial active

adaptation during cyclic loading might not have been present in E5 and S5 experiments if the force–extension tests did not exceed 5% stretch; alternatively, an active cell contribution might appear in E10 experiments if the force–extension tests surpass 10% strain. These and other hypotheses remain to be investigated by further studies.

Note that the static direction in the S5 experiments only experienced an imposed 10% change in strain seven times (once during each force–extension test), whereas both directions in the E10 experiments experienced an imposed 10% strain thousands of times. Despite this difference, the reduction in force was similar in all tested conditions, independent of boundary conditions. Note that such a force reduction is not limited to the experiments performed herein, as previous studies have shown that SMCs are unable to maintain a steady force for a prolonged time during static culture (Eichinger et al., 2020; Hall et al., 2007). Interestingly, pilot studies with 5% cyclic loading and no force–extension testing delayed the force reduction but did not prevent it compared to static experiments (data not shown). It thus appears that short-term, intermittent force–extension tests may have impacted the force reduction, but underlying mechanisms remain unclear.

It is important to note that comparing data from different studies can be complicated due to many factors. For example, a key difference compared to other studies is that the tissue equivalents tested herein were not mature. In multiple studies (Hu et al., 2013; Wagenseil et al., 2003; Walker et al., 2020; Wille et al., 2006), the tissue constructs were allowed to compact or incubate under dynamic loading (Lee et al., 2018) for several days before testing. This affects the mechanical properties of the gels and, hence, the measured forces. Another complicating factor is that different experimental designs are used to characterize the mechanical properties of the gels or to measure cell-generated forces. For instance, the shape of tissue-equivalents varies across different studies, with some using ring samples (Wagenseil et al., 2003; Wille et al., 2006), others uniaxial samples (Walker et al., 2020), and some biaxial samples, even with different geometries (Hu et al., 2013; Sander et al., 2011). Each testing method has advantages and disadvantages. The factors mentioned above, as well as differences in the experimental setup (cell type, serum concentration, preconditioning, applied stretch rate, etc.), must be kept in mind when comparing or translating results across different systems. We focused herein on different biaxial stretching protocols while maintaining the stretch rate fixed. Further studies should explore responses across multiple stretch rates as well as possible changes due to different degrees of hydration and levels of compressibility that would be expected to affect viscoelastic responses.

Whereas computational models should guide experimental design (Humphrey et al., 2008; Niklason et al., 2010), such modeling must be informed by relevant data. We submit that the present data will contribute to the development of new models for aortic smooth muscle cells and that additional theoretically motivated studies will be needed not only for VSMCs but also primary aortic fibroblasts. Indeed, these fibroblasts play a critical role in many cases of aortic remodeling, including in hypertension (Bersi et al., 2016). Again, notwithstanding the aforementioned caveats, biaxial testing should be used given the *in vivo* loading conditions on the aorta, which renders strip-biaxial testing at multiple fixed stretches informative for examining the critical role of axial loading on cell responses (Gleason and Humphrey, 2005b). Indeed, axial remodeling is often the earliest in many cases of aortic adaptation or maladaptation to perturbations in loading. Finally, the present study focused on mechanical homeostasis (Eichinger et al., 2021), but there will also be a need to design similar *ex vivo* studies to assess and/or test hypotheses regarding mechanobiological stability (Cyron and Humphrey, 2014).

5. Conclusion

This study sought to explore impacts of different mechanical constraints in combination with dynamic cyclic loading on possible biaxial tensional homeostasis in VSMC-seeded collagen-based tissue equivalents. It was observed that steady-state mean forces remained consistent across all tested conditions despite significant differences in boundary conditions and loading amplitudes. Additionally, the stiffness-force relationships assessed via equibiaxial force–extension tests showed remarkable similarity for ranges of loading to which the cells had adapted during previous cyclic loading periods. These results are consistent with prior findings of a critical role of force/tension/stress in the mechanical adaptation of VSMCs (Kanda and Matsuda, 1994; Karkhaneh Yousefi et al., 2023; Li and Xu, 2000). Further testing with additional cell types will be needed to determine whether this behavior is specific to VSMCs or generic mechanical homeostatic processes. Furthermore, testing cells with genetic defects in mechanosensory proteins, such as in the focal adhesion complex, could provide valuable insights into the dominant mechanisms at play in the observed behavior.

CRediT authorship contribution statement

Daniel Paukner: Writing – review & editing, Writing – original draft, Visualization, Methodology, Investigation, Formal analysis, Data curation, Conceptualization. **Isabella R. Jennings:** Writing – review & editing, Writing – original draft, Visualization, Methodology, Investigation, Formal analysis, Data curation, Conceptualization. **Christian J. Cyron:** Writing – review & editing, Supervision. **Jay D. Humphrey:** Writing – review & editing, Supervision, Resources, Conceptualization.

Declaration of competing interest

The authors declare that they have no known competing financial interests or personal relationships that could have appeared to influence the work reported in this paper.

Data availability

Data will be made available on request.

Appendix A. Loading conditions

Considering idealized mechanical tests can help build conceptual understanding and motivate experimental design (Humphrey et al., 2008). Fig. A.10 illustrates four loading conditions that have proven useful in studying planar tissue equivalents, often considered on a continuum scale to have coincident principal directions of stress and stretch with a zero out-of-plane stress.

Notwithstanding the intuition gained via idealized experimental situations, actual biaxial testing of cruciform samples results in complex stress and strain fields, potentially ranging from nearly uniaxial in the four arms of the sample to nearly homogeneous biaxial in the central-most region, with non-homogeneous fields between (Hu et al., 2014). In the absence of detailed material characterization and associated finite element studies, there is a need to interpret cautiously any associated experimental results based on the measured forces and globally prescribed stretches. Consistent with other studies (Gould et al., 2012; Hu et al., 2014; Sander et al., 2011), here we provide simple illustrative finite element simulations using ABAQUS (Dassault Systems) to appreciate better the non-homogeneous fields that can develop in a biaxially tested cruciform gel (Figs. A.11 and A.12). Because of double-symmetry, only one-quarter of the cruciform geometry was modeled with corresponding symmetry boundary conditions. The domain was discretized with 1780 finite elements (C3D8H) and described by an isotropic, linear elastic material with material parameters E (Young's modulus) and ν (Poisson's ratio). E and ν were adjusted to approximate the force amplitudes measured in acellular gels under 5% equi- and strip-biaxial loading in the steady state (Fig. B.14A), as well as the amplitude ratios of the static and perturbed axis in the strip-biaxial experiments in the steady state (Fig. 4B). This resulted in a Young's

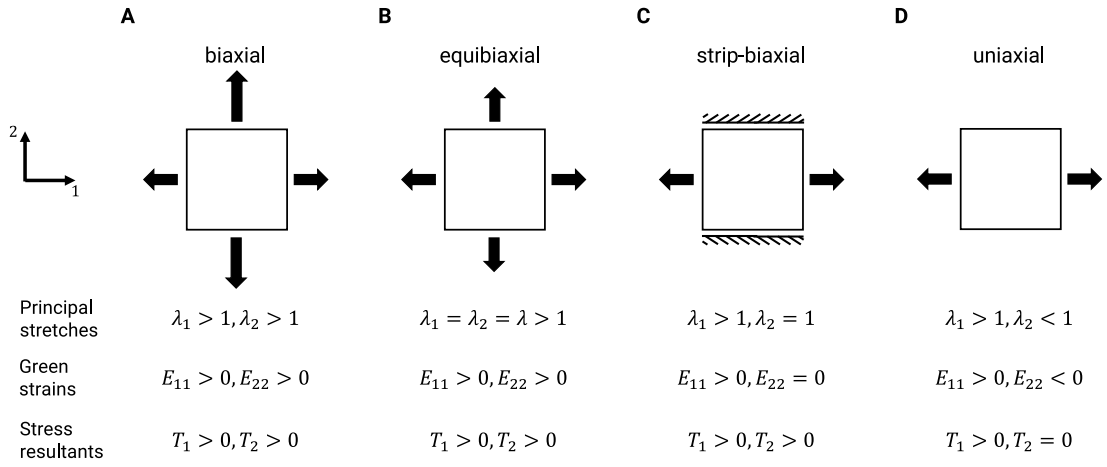

Fig. A.10. Illustration of different idealized loading conditions. (A) shows a general in-plane tensile test with biaxial stretches (λ_1, λ_2) greater than unity and associated non-negative biaxial strains and stress resultants (i.e., quantities having units of force/length that can be obtained by integrating the associated stress through the thickness). Different specializations follow in B-D. Cases (B) and (C) are relevant herein for the central region of a cruciform sample, whereas case (D) is relevant herein for the arms of a cruciform sample. It is noted further that other strip-biaxial tests could include non-zero but fixed values of E_{22}, for which the associated values of T_2 would increase further above baseline during testing.

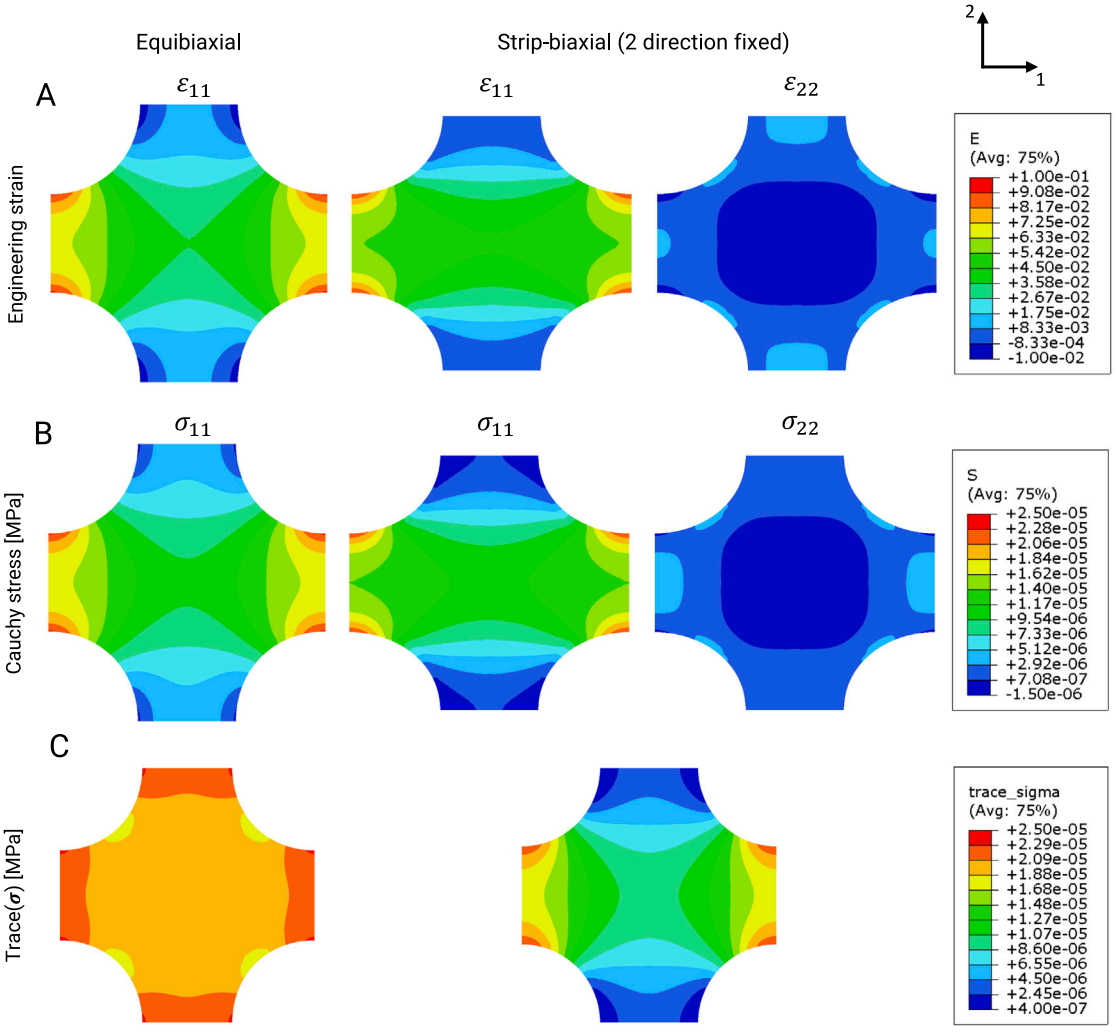

Fig. A.11. Illustrative finite element results for biaxial strains (top row) and stresses (middle and bottom rows) in a cruciform sample ($E = 250$ Pa, $\nu = 0.1$) subjected to displacement boundary conditions at the ends of the four arms. Note that, on average, the 1 and 2 directions in the equibiaxial case (left column) experience a 5% strain, while in the strip-biaxial case, the 1 direction experiences a 5% strain (middle column) and the 2 direction 0% strain (right column). Despite achieving the target levels of biaxial strain, on average, note the complex nonuniform strain and stress fields. In particular, the strain in the 2 direction yields a 2-direction stress that is both tensile (in the arms) and compressive (in the central region), though overall positive (middle row). Finally, note that coordinate invariant measures of the biaxial state of stress (bottom row), including the trace (shown) and the magnitude (not shown, but similar), reveal a more uniform distribution except for deviations in the strip-biaxial arms.

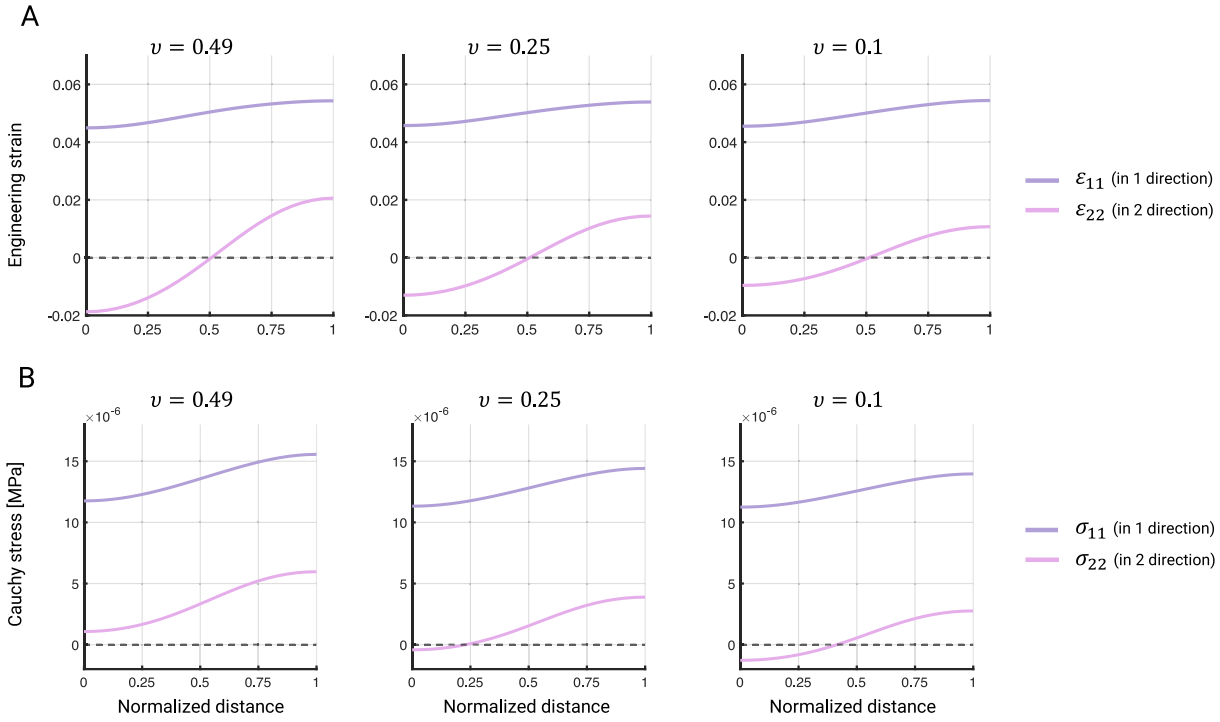

Fig. A.12. Given the idealized quarter-symmetry, illustrative biaxial strain (top) and stress (bottom) distributions along the mid-line 1 (stretched) and 2 (fixed) directions reveal that the desired strains (5% in 1 direction, 0% in 2 direction) were achieved in the strip-biaxial test, on average, when examining the full computational domain, from which the experimentally measured forces derived. Reducing the Poisson's ratio has a marked impact on the strain and stress distributions in these strip-biaxial simulations; it reduces the magnitude of the 2-direction strains, and the 2-direction stresses become slightly more compressive in the central region. Despite both tensile and compressive stresses in the 2 direction, the net stress was yet tensile in both the 1 and 2 directions as expected in a strip-biaxial test. Although cell responses likely depend on the local, not overall, state of stress and/or strain, the experimental measurement of biaxial force generation necessarily results from the integrated responses of all cells over the entire experimental domain.

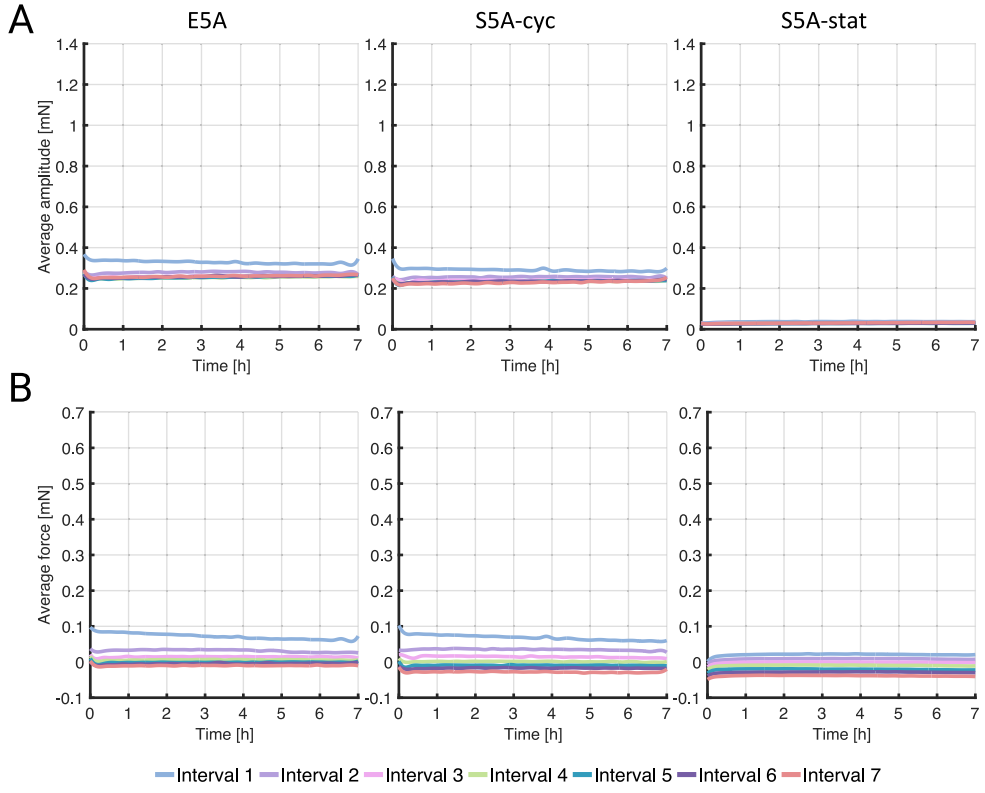

Fig. B.13. Time-averaged forces in acellular experiments during cyclic loading intervals. (A) Average force amplitude across all acellular experiments for each loading condition during the seven intervals. (B) Average mean force across all acellular experiments for each loading condition during the seven intervals. See Table 1 for the nomenclature for all testing protocols.

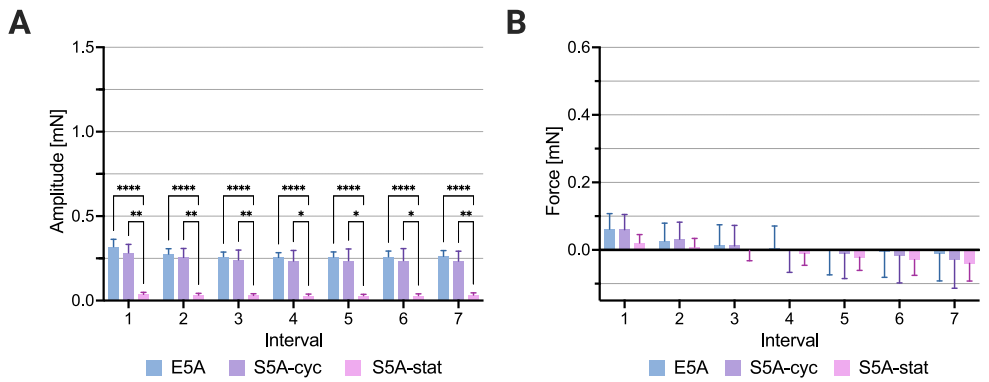

Fig. B.14. Evolution of steady-state forces in acellular experiments. (A) Force amplitudes were constant over time, with the amplitude of the static axis in the strip-biaxial being significantly different from the other amplitudes. (B) The steady-state mean forces in acellular gels were low and showed a slight decrease over time. (*$p < 0.05$, **$p < 0.01$, ***$p < 0.001$, ****$p < 0.0001$) See Table 1 for the nomenclature for all testing protocols.

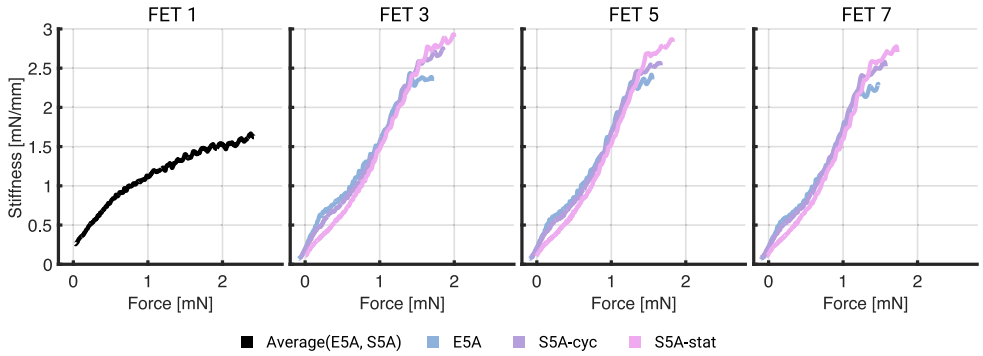

Fig. B.15. Stiffness-force relationship for acellular experiments during selected force–extension tests (FETs). All gels exhibited a similar behavior during the first test, which did not change as significantly as cell-seeded gels in the following tests. The stiffness-force relationship remained approximately linear throughout all the force–extension tests. Black – Average of the first force–extension test in E5A, S5A-cyc, and S5A-stat experiments, blue – average of E5A experiments, purple – average of S5A-cyc experiments, pink – average of S5A-stat experiments. See Table 1 for the nomenclature for all testing protocols.

modulus of 250 Pa and a Poisson's ratio of 0.1, which are comparable to previously measured values of acellular collagen gels (Raub et al., 2010). Figs. A.11 and A.12 show strain and stress distributions for the equibiaxial case (prescribed 5% strain in the 1 and 2 direction) and strip-biaxial case (prescribed 5% strain in the 1 direction, 0% strain in the 2 direction). Because of the isotropy and the symmetric loading in the equibiaxial case, only the strains and stresses in the 1 direction are shown.

Appendix B. Acellular experiments

See Figs. B.13–B.15.

References

Bäck, M., Gasser, T.C., Michel, J.-B., Caligiuri, G., 2013. Biomechanical factors in the biology of aortic wall and aortic valve diseases. Cardiovasc. Res. 99 (2), 232–241. http://dx.doi.org/10.1093/cvr/cvt040.

Barocas, V.H., Tranquillo, R.T., 1997. An anisotropic biphasic theory of tissue-equivalent mechanics: the interplay among cell traction, fibrillar network deformation, fibril alignment, and cell contact guidance. J. Biomech. Eng. 119 (2), 137–145. http://dx.doi.org/10.1115/1.2796072.

Bell, E., Ivarsson, B., Merrill, C., 1979. Production of a tissue-like structure by contraction of collagen lattices by human fibroblasts of different proliferative potential in vitro. Proc. Natl. Acad. Sci. 76 (3), 1274–1278. http://dx.doi.org/10.1073/pnas.76.3.1274.

Bersi, M.R., Bellini, C., Wu, J., Montaniel, K.R., Harrison, D.G., Humphrey, J.D., 2016. Excessive adventitial remodeling leads to early aortic maladaptation in angiotensin-induced hypertension. Hypertension 67 (5), 890–896. http://dx.doi.org/10.1161/HYPERTENSIONAHA.115.06262.

Brown, R.A., Prajapati, R., McGrouther, D.A., Yannas, I.V., Eastwood, M., 1998. Tensional homeostasis in dermal fibroblasts: Mechanical responses to mechanical loading in three-dimensional substrates. J. Cell. Physiol. 175 (3), 323–332. http://dx.doi.org/10.1002/(SICI)1097-4652(199806)175:3<323::AID-JCP10>3.0.CO;2-6.

Chen, K., Vigliotti, A., Bacca, M., McMeeking, R.M., Deshpande, V.S., Holmes, J.W., 2018. Role of boundary conditions in determining cell alignment in response to stretch. Proc. Natl. Acad. Sci. 115 (5), 986–991. http://dx.doi.org/10.1073/pnas.1715059115.

Cyron, C., Humphrey, J., 2014. Vascular homeostasis and the concept of mechanobiological stability. Internat. J. Engrg. Sci. 85, 203–223. http://dx.doi.org/10.1016/j.ijengsci.2014.08.003.

Eichinger, J.F., Haeusel, L.J., Paukner, D., Aydin, R.C., Humphrey, J.D., Cyron, C.J., 2021. Mechanical homeostasis in tissue equivalents: a review. Biomech. Model. Mechanobiol. 20 (3), 833–850. http://dx.doi.org/10.1007/s10237-021-01433-9.

Eichinger, J.F., Paukner, D., Szafron, J.M., Aydin, R.C., Humphrey, J.D., Cyron, C.J., 2020. Computer-controlled biaxial bioreactor for investigating cell-mediated homeostasis in tissue equivalents. J. Biomech. Eng. 142 (7), http://dx.doi.org/10.1115/1.4046201.

Engler, A.J., Sen, S., Sweeney, H.L., Discher, D.E., 2006. Matrix elasticity directs stem cell lineage specification. Cell 126 (4), 677–689. http://dx.doi.org/10.1016/j.cell.2006.06.044.

Ezra, D.G., Ellis, J.S., Beaconsfield, M., Collin, R., Bailly, M., 2010. Changes in fibroblast mechanostat set point and mechanosensitivity: an adaptive response to mechanical stress in floppy eyelid syndrome. Investig. Opthalmology Vis. Sci. 51 (8), 3853. http://dx.doi.org/10.1167/iovs.09-4724.

Ferruzzi, J., Bersi, M.R., Humphrey, J.D., 2013. Biomechanical phenotyping of central arteries in health and disease: advantages of and methods for murine models. Ann. Biomed. Eng. 41 (7), 1311–1330. http://dx.doi.org/10.1007/s10439-013-0799-1.

Gleason, R., Humphrey, J., 2005a. Effects of a sustained extension on arterial growth and remodeling: a theoretical study. J. Biomech. 38 (6), 1255–1261. http://dx.doi.org/10.1016/j.jbiomech.2004.06.017.

Gleason, R.L., Humphrey, J.D., 2005b. A 2D constrained mixture model for arterial adaptations to large changes in flow, pressure and axial stretch. Math. Med. Biol.: J. IMA 22 (4), 347–369. http://dx.doi.org/10.1093/imammb/dqi014.

Gould, R.A., Chin, K., Santisakultarm, T.P., Dropkin, A., Richards, J.M., Schaffer, C.B., Butcher, J.T., 2012. Cyclic strain anisotropy regulates valvular interstitial cell

phenotype and tissue remodeling in three-dimensional culture. Acta Biomater. 8 (5), 1710–1719. http://dx.doi.org/10.1016/j.actbio.2012.01.006.

Hall, S.M., Soueid, A., Smith, T., Brown, R.A., Haworth, S.G., Mudera, V., 2007. Spatial differences of cellular origins and in vivo hypoxia modify contractile properties of pulmonary artery smooth muscle cells: lessons for arterial tissue engineering. J. Tissue Eng. Regen. Med. 1 (4), 287–295. http://dx.doi.org/10.1002/term.39.

Hu, J.-J., Chen, G.-W., Liu, Y.-C., Hsu, S.-S., 2014. Influence of specimen geometry on the estimation of the planar biaxial mechanical properties of cruciform specimens. Exp. Mech. 54 (4), 615–631. http://dx.doi.org/10.1007/s11340-013-9826-2.

Hu, J.-J., Humphrey, J.D., Yeh, A.T., 2009. Characterization of engineered tissue development under biaxial stretch using nonlinear optical microscopy. Tissue Eng. Part A 15 (7), 1553–1564. http://dx.doi.org/10.1089/ten.tea.2008.0287.

Hu, J.-J., Liu, Y.-C., Chen, G.-W., Wang, M.-X., Lee, P.-Y., 2013. Development of fibroblast-seeded collagen gels under planar biaxial mechanical constraints: a biomechanical study. Biomech. Model. Mechanobiol. 12 (5), 849–868. http://dx.doi.org/10.1007/s10237-012-0448-x.

Humphrey, J.D., Dufresne, E.R., Schwartz, M.A., 2014. Mechanotransduction and extracellular matrix homeostasis. Nat. Rev. Mol. Cell Biol. 15 (12), 802–812. http://dx.doi.org/10.1038/nrm3896.

Humphrey, J.D., Eberth, J.F., Dye, W.W., Gleason, R.L., 2009. Fundamental role of axial stress in compensatory adaptations by arteries. http://dx.doi.org/10.1016/j.jbiomech.2008.11.011.

Humphrey, J.D., Wells, P.B., Baek, S., Hu, J.-J., McLeroy, K., Yeh, A.T., 2008. A theoretically-motivated biaxial tissue culture system with intravital microscopy. Biomech. Model. Mechanobiol. 7 (4), 323–334. http://dx.doi.org/10.1007/s10237-007-0099-5.

Hynes, R.O., Naba, A., 2012. Overview of the matrisome – an inventory of extracellular matrix constituents and functions. Cold Spring Harb. Perspect. Biol. 4 (1), a004903. http://dx.doi.org/10.1101/cshperspect.a004903.

Jhun, C.-S., Evans, M.C., Barocas, V.H., Tranquillo, R.T., 2009. Planar biaxial mechanical behavior of bioartificial tissues possessing prescribed fiber alignment. J. Biomech. Eng. 131 (8), http://dx.doi.org/10.1115/1.3148194.

Kanda, K., Matsuda, T., 1994. Mechanical stress-induced orientation and ultrastructural change of smooth muscle cells cultured in three-dimensional collagen lattices. Cell Transplant. 3 (6), 481–492. http://dx.doi.org/10.1177/096368979400300605.

Karkhaneh Yousefi, A.A., Petit, C., Ben Hassine, A., Avril, S., 2023. Stiffness sensing by smooth muscle cells: Continuum mechanics modeling of the acto-myosin role. J. Mech. Behav. Biomed. Mater. 144, 105990. http://dx.doi.org/10.1016/j.jmbbm.2023.105990.

Klein, E.A., Yin, L., Kothapalli, D., Castagnino, P., Byfield, F.J., Xu, T., Levental, I., Hawthorne, E., Janmey, P.A., Assoian, R.K., 2009. Cell-cycle control by physiological matrix elasticity and in vivo tissue stiffening. Curr. Biol. 19 (18), 1511–1518. http://dx.doi.org/10.1016/j.cub.2009.07.069.

Lee, P.-Y., Liu, Y.-C., Wang, M.-X., Hu, J.-J., 2018. Fibroblast-seeded collagen gels in response to dynamic equibiaxial mechanical stimuli: A biomechanical study. J. Biomech. 78, 134–142. http://dx.doi.org/10.1016/j.jbiomech.2018.07.030.

Li, C., Xu, Q., 2000. Mechanical stress-initiated signal transductions in vascular smooth muscle cells. Cell. Signal. 12 (7), 435–445. http://dx.doi.org/10.1016/S0898-6568(00)00096-6.

Lukashev, M., 1998. ECM signalling: orchestrating cell behaviour and misbehaviour. Trends Cell Biol. 8 (11), 437–441. http://dx.doi.org/10.1016/S0962-8924(98)01362-2.

Mol, A., Driessen, N.J.B., Rutten, M.C.M., Hoerstrup, S.P., Bouten, C.V.C., Baaijens, F.P.T., 2005. Tissue engineering of human heart valve leaflets: a novel bioreactor for a strain-based conditioning approach. Ann. Biomed. Eng. 33 (12), 1778–1788. http://dx.doi.org/10.1007/s10439-005-8025-4.

Niklason, L.E., Yeh, A.T., Calle, E.A., Bai, Y., Valentín, A., Humphrey, J.D., 2010. Enabling tools for engineering collagenous tissues integrating bioreactors, intravital imaging, and biomechanical modeling. Proc. Natl. Acad. Sci. 107 (8), 3335–3339. http://dx.doi.org/10.1073/pnas.0907813106.

Proudfoot, D., Shanahan, C., 2012. Human vascular smooth muscle cell culture. In: Mitry Ragai, R., Hughes, R.D. (Eds.), Human Cell Culture Protocols. Humana Press, Totowa, NJ, pp. 251–263. http://dx.doi.org/10.1007/978-1-61779-367-7{_}17.

Raub, C., Putnam, A., Tromberg, B., George, S., 2010. Predicting bulk mechanical properties of cellularized collagen gels using multiphoton microscopy. Acta Biomater. 6 (12), 4657–4665. http://dx.doi.org/10.1016/j.actbio.2010.07.004.

Redden, R.A., Doolin, E.J., 2003. Collagen crosslinking and cell density have distinct effects on fibroblast-mediated contraction of collagen gels. Skin Res. Technol. 9 (3), 290–293. http://dx.doi.org/10.1034/j.1600-0846.2003.00023.x.

Sander, E.A., Barocas, V.H., Tranquillo, R.T., 2011. Initial fiber alignment pattern alters extracellular matrix synthesis in fibroblast-populated fibrin gel cruciforms and correlates with predicted tension. Ann. Biomed. Eng. 39 (2), 714–729. http://dx.doi.org/10.1007/s10439-010-0192-2.

Seliktar, D., Nerem, R.M., Galis, Z.S., 2001. The role of matrix metalloproteinase-2 in the remodeling of cell-seeded vascular constructs subjected to cyclic strain. Ann. Biomed. Eng. 29 (11), 923–934. http://dx.doi.org/10.1114/1.1415522.

Shearn, J.T., Juncosa-Melvin, N., Boivin, G.P., Galloway, M.T., Goodwin, W., Gooch, C., Dunn, M.G., Butler, D.L., 2007. Mechanical stimulation of tendon tissue engineered constructs: effects on construct stiffness, repair biomechanics, and their correlation. J. Biomech. Eng. 129 (6), 848–854. http://dx.doi.org/10.1115/1.2800769.

Simon, D., Niklason, L., Humphrey, J., 2014. Tissue transglutaminase, not lysyl oxidase, dominates early calcium-dependent remodeling of fibroblast-populated collagen lattices. Cells Tissues Organs 200 (2), 104–117. http://dx.doi.org/10.1159/000381015.

Thomopoulos, S., Fomovsky, G.M., Holmes, J.W., 2005. The development of structural and mechanical anisotropy in fibroblast populated collagen gels. J. Biomech. Eng. 127 (5), 742–750. http://dx.doi.org/10.1115/1.1992525.

Wagenseil, J.E., Wakatsuki, T., Okamoto, R.J., Zahalak, G.I., Elson, E.L., 2003. One-dimensional viscoelastic behavior of fibroblast populated collagen matrices. J. Biomech. Eng. 125 (5), 719–725. http://dx.doi.org/10.1115/1.1614818.

Walker, M., Rizzuto, P., Godin, M., Pelling, A.E., 2020. Structural and mechanical remodeling of the cytoskeleton maintains tensional homeostasis in 3D microtissues under acute dynamic stretch. Sci. Rep. 10 (1), 7696. http://dx.doi.org/10.1038/s41598-020-64725-7.

Wang, H.-B., Dembo, M., Wang, Y.-L., 2000. Substrate flexibility regulates growth and apoptosis of normal but not transformed cells. Am. J. Physiol. Cell Physiol. 279 (5), C1345–C1350. http://dx.doi.org/10.1152/ajpcell.2000.279.5.C1345.

Wells, R.G., 2008. The role of matrix stiffness in regulating cell behavior. Hepatology 47 (4), 1394–1400. http://dx.doi.org/10.1002/hep.22193.

Wille, J.J., Elson, E.L., Okamoto, R.J., 2006. Cellular and matrix mechanics of bioartificial tissues during continuous cyclic stretch. Ann. Biomed. Eng. 34 (11), 1678–1690. http://dx.doi.org/10.1007/s10439-006-9153-1.

Wolf, K., te Lindert, M., Krause, M., Alexander, S., te Riet, J., Willis, A.L., Hoffman, R.M., Figdor, C.G., Weiss, S.J., Friedl, P., 2013. Physical limits of cell migration: control by ECM space and nuclear deformation and tuning by proteolysis and traction force. J. Cell Biol. 201 (7), 1069–1084. http://dx.doi.org/10.1083/jcb.201210152.

Yamada, K.M., Doyle, A.D., Lu, J., 2022. Cell–3D matrix interactions: recent advances and opportunities. Trends Cell Biol. 32 (10), 883–895. http://dx.doi.org/10.1016/j.tcb.2022.03.002.